Geophysical Journal International

Geophys. J. Int. (2010) **183,** 163–177 doi: 10.1111/j.1365-246X.2010.04736.x

Magnetic mineral inventory of equatorial Atlantic Ocean marine sediments off Senegal—glacial and interglacial contrast

Achakie Cletus Itambi,[1,2] Tilo von Dobeneck,[1,2] Mark J. Dekkers[3] and Thomas Frederichs[1]

[1]*Department of Geosciences, University of Bremen, Klagenfurter Str.,* D-28359 *Bremen, Germany. E-mail: itambijr@yahoo.com*
[2]*Center for Marine Environmental Sciences, University of Bremen, Leobener Str.,* D-28359 *Bremen, Germany*
[3]*Paleomagnetic Laboratory Fort Hoofddijk, Utrecht University, Budapestlaan* 17, 3584 *CD Utrecht, the Netherlands*

Accepted 2010 July 12. Received 2010 July 6; in original form 2009 May 27

SUMMARY

In complex sedimentary environments with different sources of the magnetic particles, it is vital that all factors contributing to and affecting the magnetic signals be well understood for a better constrained interpretation of palaeomagnetic and climatic data. Palaeoclimatically driven signals may be convolved with volcanic and cosmogenic sources, and diagenesis may alter the primary magnetic mineral assemblage. Rock magnetic methods and electron microscopy provide suitable means to characterize magnetic assemblages. In this study of core-retrieved sediments from the last 150 kyr off the coast of Senegal (NW Africa), the occurrence of magnetic spherules of volcanic origin and cosmogenic particles appeared to be insignificant. In glacial stages, ferrimagnetic iron and iron-titanium oxides magnetically dominate with few signs of a diagenetic overprint. Low- and room temperature magnetic results reveal evidence for haematite and goethite while haemoilmenite and titanomagnetite were identified from low-temperature AC susceptibility measurements and SEM observations. In contrast, the interglacial samples appeared to have been severely affected by diagenesis, with pyrite making up over 50 per cent of the iron-bearing phases. The Verwey transition observed at 110 K confirms the presence of magnetite. The glacial and interglacial contrast reveals the close link between northwest African climate and the magnetic mineralogy of the sediments.

Key words: Environmental magnetism; Magnetic mineralogy and petrology; Rock and mineral magnetism.

1 INTRODUCTION

Marine sedimentary environments are often complex because of the large number of potential sources of magnetic minerals. Presumably, climatically regulated sources not only include detrital minerals that reflect weathering and erosion on land, but also post-depositional processes like diagenesis, authigenesis and biomineralization are in a sense climatically driven (Karlin & Levi 1983; Robinson 1986; von Dobeneck *et al.* 1987; Suk *et al.* 1990) via the amount of organic matter, sedimentation and redox conditions. Volcanic material (Freeman 1986) and cosmic particles (Brownlow *et al.* 1966; Brownlee 1981) are other potential sources which may contribute significantly to, and in some cases, be the dominant carriers of the magnetic signature in the sediments. Therefore, the interpretation of rock and palaeomagnetic results is not always straightforward. Possible ambiguity is reduced by investigation of mineral magnetic properties at high fields and at low and high temperature and by utilizing microscopy (electron) to visualize the magnetic particles that are responsible for the measured magnetic properties. This study involves this type of analysis on a sediment core from off the Senegal continental margin (Fig. 1a).

The Senegal continental margin is situated at the northern summer limit of the Intertropical Convergence Zone, that is, the boundary between humid and arid North Africa. It receives detrital sediments via fluvial (Gac & Kane 1986a,b) and aeolian pathways (Bloemendal *et al.* 1988; Balsam *et al.* 1995). The northwest African margin is also characterized by high marine productivity. Average sedimentation rates of ∼8 cm kyr^{-1} were found off Senegal at about 3000 m water depth (Itambi *et al.* 2009). This may create microphylic conditions suitable for reductive diagenesis and biomineralization. A magnetically complex sedimentary environment may well be the overall result.

Bloemendal *et al.* (1988) were among the first to show climate-driven variations in magnetic mineral fluxes in this region. They documented that glacials were marked by a higher concentration of magnetic minerals, mostly dominated by single domain (SD) and pseudo-single-domain (PSD) magnetite as well as a significant proportion of haematite and goethite, whereas, the warmer interglacials were characterized by enhanced input of superparamagnetic (SP) magnetite. This conflicts with our recent findings (Itambi *et al.* 2009), which tend to identify a very high concentration of SP particles (frequency dependence of susceptibility

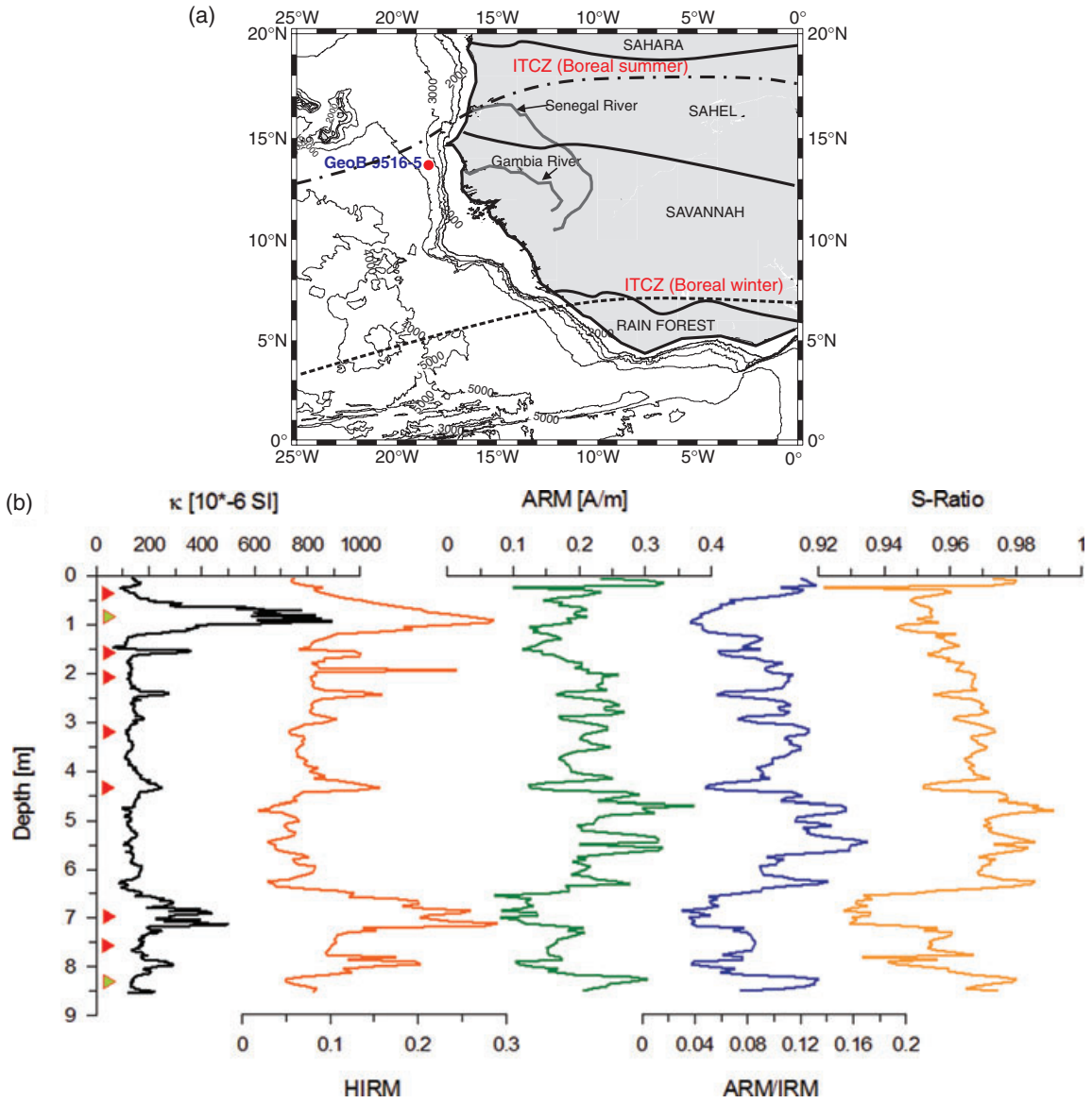

Figure 1. (a) Location of core GeoB 9516–5 off coast Senegal recovered at 3500 m water depth. The solid line indicates the present day summer northern limit of the tropical rain belt (ITCZ) while the dashed lines show its winter position. (b) Down core profiles of the magnetic parameters (Itambi *et al.* 2009) indicating the intervals that were sampled (arrow heads), and those that are presented in this study (Green arrow heads).

>12 per cent) during extreme glacial events (Heinrich-like events) and an SD magnetite-dominated interglacial. The SP particles correlate to the 'hard' isothermal remanent magnetization (HIRM in Itambi *et al.* (2009)) and low-field susceptibility. Moreover intervals identified from diffuse reflectance spectrophotometry as enriched in haematite and goethite have a larger amount of SP particles. This prompted Itambi *et al.* (2009) to suggest the presence of ultrafine-grained haematite and goethite as coatings on quartz grains.

It is therefore imperative that studies be carried out in this seemingly complex sedimentary environment with several potential sources for the magnetic mineral assemblage, to identify the magnetic mineral phases, distinguish the relative contribution of each mineral and grain-size class to the magnetic properties, for a better constrained interpretation of palaeomagnetic, environmental and climatic results. This study will seek to constrain observations and inferences put forward in Itambi *et al.* (2009). To achieve this, we perform several more specialized rock magnetic measurements capable of distinguishing between magnetic mineral phases. These include determination of the remanence behaviour at low temperature, acquisition of thermomagnetic data with a Curie balance, and determination of first-order reversal curves (FORCs) diagrams and isothermal remanent magnetization (IRM) acquisition curves. Since no single technique is able to fully characterize the sediment, we also applied scanning electron microscopy (SEM) in addition to the mineral magnetic analysis. The results show a magnetic mineral assemblage consisting of the full range of detrital, authigenic, diagenetic and possible cosmic provenance. Pyrite, which indicates a reducing or anoxic environment, was abundant as well as some reoxidized magnetic particles of secondary origin.

2 MATERIALS AND METHODS

During the research cruise M61 (Mulitza *et al.* 2006) off northwest Africa, sediment cores depicting an alternating sequence of

reddish brown and dark green layers were recovered. Itambi *et al.* (2009), analysed the climatic records of some of these cores, that is, GeoB 9506-1, GeoB 9516-5 and GeoB 9527-5, and reported magnetic signals that followed glacial and interglacial patterns synchronous with the colour changes. The reddish brown glacial intervals demonstrated a higher concentration of magnetic minerals, as was reflected in the magnetic susceptibility ($150 \leq \kappa \leq 800 \times 10^{-6}$ SI), and SIRM. The dark green interglacial layers showed lower concentration ($100 \leq \kappa \leq 150 \times 10^{-6}$ SI); SIRM was equally lower. For this reason, nine samples were selected from these two lithological units at different depth intervals from core GeoB 9516-5 (Fig. 1a) and studied here in considerably more detail. Since the nine samples tend to be representative of the two climatic periods, we focus our analysis and discussion in this paper on two of the samples, one from each lithology (Fig. 1b). The glacial sample was recovered at 85 cm core depth while the interglacial sample was taken at 836 cm depth.

2.1 Magnetic and heavy liquid extraction

The magnetic minerals were extracted for SEM and magnetic properties measuring system (MPMS) analysis. Two extraction methods were used, that is, magnetic extraction method described by Petersen *et al.* (1986) and von Dobeneck *et al.* (1987); and heavy liquid separation (HLS) proposed by Franke *et al.* (2007a) that separated the iron minerals from the rest of the sediment components based on their higher density. As demonstrated by Franke *et al.* (2007a), magnetic extraction has the potential to extract larger quantities of magnetic minerals but tends to be biased with respect to the coarser particles. HLS also includes non-magnetic phases such as iron sulphides since the separation is highly dependent on the density of the particles. To enhance the concentration of magnetic minerals from the HLS, a portion of the extract was dispersed again with demineralized water in a small glass vial and a 'magnetic finger' (*cf.* Petersen *et al.* (1986)) was used to attract the magnetic component. After separation, the extracts were stored in glass vials filled with ethanol until further processing (usually between two and four days).

2.2 Magnetic measurements at room temperature

These measurements involved the determination of acquisition curves of the IRM in fields up to 7 Tesla and determination of FORCs (Pike *et al.* 1999; Roberts *et al.* 2000). The IRM was measured on magnetic extracts using the Quantum Design Magnetic Properties Measurement System (MPMS-XL-2) SQUID magnetometer at the Marine Geophysics Department of the University of Bremen (Germany). IRM acquisition curves were processed with the software described by Kruiver *et al.* (2001) that is based on fitting of lognormal coercivity distributions. FORC diagrams were acquired with an Alternating Gradient Magnetometer Model 2900 (MicroMag, Princeton, USA) at Utrecht University, to determine the domain-state of the particles. Bulk sediments of about 25 mg were put into a 0.5-cm straw, sealed with non-magnetic glue and were mounted on a P1 parallel silica probe for measurements. A total of 200 FORCs were measured per sample at a field increment of 0.984 mT, the saturation field was 2 T and the averaging time was 0.1 s. Since both samples exhibited low coercivities, a maximum field of 120 mT was applied. The data was processed using Harrison–Feinberg algorithm—FORCINEL (Harrison & Feinberg 2008).

2.3 Magnetic measurements below and above room temperature

Low-temperature remanence measurements were performed on bulk samples as well as separates using the MPMS. The samples were weighted (20–50 mg) and then put into gelatine capsules, which were inserted and firmly held in plastic straws. AC magnetic susceptibility was first measured at four different frequencies (1, 10, 100 and 1000 Hz) during warming from 5 to 300 K in a field of 0.04 mT. The samples were afterwards cooled in the absence of a field (zero-field-cooled, ZFC) to 5 K where an IRM was imparted in a field of 7 T. The remanent magnetization was measured during zero field warming from 5 K to room temperature (300 K) at 2 K increments. The samples were again cooled but this time in an applied field of 7 T (field-cooled, FC) which was switched off at 5 K before warming to 300 K. Furthermore, an (S)IRM was cycled by cooling through 300–5 K and then gradually warmed back through the same temperature range. The remanence was continually measured at ∼2 K intervals during the entire cycling.

Thermomagnetic analysis above room temperature was performed on a modified horizontal translation Curie balance (Mullender *et al.* 1993) at the palaeomagnetic laboratory 'Fort Hoofddijk', Utrecht University (The Netherlands). Samples were heated in air in a cycling field between 150 and 300 mT to a maximum temperature of 700 °C at a heating and cooling rate of 10 °C min^{-1}. To investigate chemical alteration, we employed the incremental heating and cooling segment protocol. This involved heating the samples to a certain temperature, cooling it down to a chosen value (typically 80–100 °C lower), and then heating and cooling repeatedly to increasingly higher temperatures until the maximum temperature of 700 °C is attained.

2.4 Scanning Electron Microscopy

Portions of the HLS concentrate (up to ∼15 mg) were allowed to dry in air and the samples were spread on a carbon sticker. This was sputtered with carbon for SEM and accompanying Energy Dispersive X-ray spectroscopy analysis (EDS). The SEM instrument used is the SUPRA™ 40 high-resolution FESEM based on the third generation GEMINI column by Carl Zeiss SMT. Secondary electron (SE) imaging was used at energy levels between 5 and 15 kV. For elemental composition, the EDS attached to the instrument was used and the applied energy for this analysis was 15 kV. The elemental spectra were normalized by their oxygen values.

3 RESULTS

3.1 Rock magnetic results

3.1.1 IRM acquisition at room temperature

IRM acquisition was performed on magnetic extracts. The glacial sample (Fig. 2a) acquires about 65 per cent of its total 7 T remanence at 200 mT and continues to acquire remanence at 7 T. In the interglacial sample (Fig. 2b), up to 90 per cent of its 7 T IRM was acquired at ∼200 mT, even though IRM acquisition continued at 7 T. To assess the magnetic mineral phases contributing to the IRM, IRM component analysis (Kruiver *et al.* 2001) was done (Fig. 2 and Table 1). A total of three components were identified for the glacial sample (Figs 2a, c and e). Component 1 with a remanent acquisition coercive force ($B_{1/2}$) of ∼40 mT and a dispersion parameter (DP) of 0.35 log mT shows the highest contribution to the

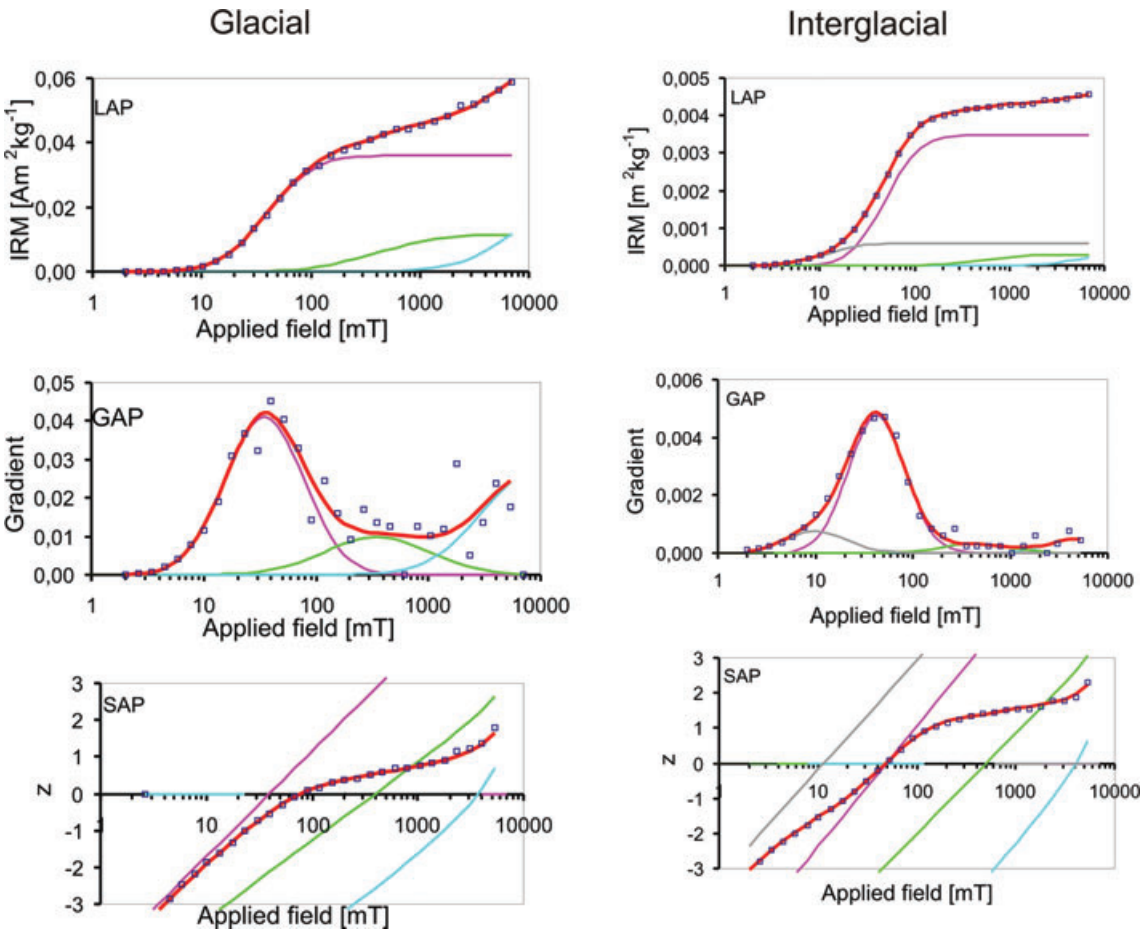

Figure 2. IRM acquisition curves with the results of component analysis. LAP = linear acquisition plots, GAP = gradient acquisition plots and SAP = standardized acquisition plot. Dots are data points while the red line shows the best fit. In the glacial sample, the colours purple, green and blue represent magnetite, haematite and goethite, respectively. In the interglacial sample, the same colours represent magnetite, goethite and haematite, respectively while the grey line shows 'soft' magnetite.

Table 1. Results of the IRM component analysis.

Component	SIRM (Am^2 kg^{-1})	SIRM (per cent)	Log ($B_{1/2}$)	$B_{1/2}$ mT	DP mT
Glacial					
1	0.036	43.6	1.6	39.8	0.35
2	0.0115	13.9	2.6	398	0.47
3	0.035	42.5	4.06	11481	0.50
Interglacial					
1	3.47×10^{-3}	73.1	1.69	49	0.29
2	4.0×10^{-4}	8.4	3.8	6309	0.32
3	2.8×10^{-4}	5.9	2.7	501	0.35
4	6.0×10^{-4}	12.6	1.06	11	0.32

IRM (~43.6 per cent, Table 1). This soft component is interpreted as magnetite. In the second component (component 2) the $B_{1/2}$ is ~400 mT, which is in the range of the B1/2 of haematite. This component has the smallest contribution to the acquisition curve, with a 13.9 per cent fraction. For the third component, (component 3), the $B_{1/2}$ is very high (~11.5 T), a strong indication that it is the high-coercivity mineral goethite. This component contributes ~42.5 per cent of the remanence. Since the IRM was only acquired up to 7 T, the high $B_{1/2}$ for component 3 is an extrapolation based on the log-Gaussian curve shape fitted to each component.

The interglacial sample yielded four components (Figs 2b, d and f) with marked differences in comparison to the glacial sample. Component 1, which contributes ~73 per cent to the remanence and is interpreted as magnetite based on its $B_{1/2}$, has a higher coercivity ($B_{1/2}$ ~49 mT) and a narrower DP (0.29) compared to the equivalent component in the glacial sample. The harder magnetite could be indicative of low-temperature oxidation (partial maghemitization; e.g. Petersen & Vali 1987; Van Velzen & Dekkers 1999). Component 2, which has a $B_{1/2}$ representative of goethite (~6.3 T) and DP of 0.32, is the second dominant

component with an ∼8.5 per cent contribution to the remanence. The third component is interpreted as haematite, with a $B_{1/2}$ ∼500 mT and a DP of 0.35 mT and contributes ∼6 per cent. 'Component 4' is a very soft component with a $B_{1/2}$ of 11.5 mT and DP of 0.32 and a total contribution of 12.6 per cent. This component is a consequence of the symmetric base function that is mandatory in this fitting package. Small grains show a skewed-to-the-left distribution (Egli 2004), which cannot be fitted. Proper fitting requires a second distribution, which has no physical meaning. As observed, magnetite is the dominant contributor in all samples, but its dominance is much greater in the interglacial sample where it contributes over two-thirds of the SIRM. High-coercivity minerals haematite and goethite make up a more significant proportion in the glacial sample.

3.1.2 First-order-reversal curves

FORCs distributions (acquired on bulk material) for the two climatic periods show distinct features (Fig. 3). The central contours around the most prominent density maxima centred at Bc ∼12 and Bu 0 mT (glacial) and ∼26 and 0 mT (interglacial) are mostly closed, which complies with SD magnetite (Roberts *et al.* 2000). Both samples also show very little contour spreading on the Bu axis indicating that magnetic interaction is not important (Pike *et al.* 1999; Roberts *et al.* 2000). Glacial sediments are characterized by two maxima in the FORC density (Fig. 3a) while the interglacial sample shows only one.

Close to the ordinate axis, the FORC diagram of the glacial sample is characterized by diverging contours indicative of fine

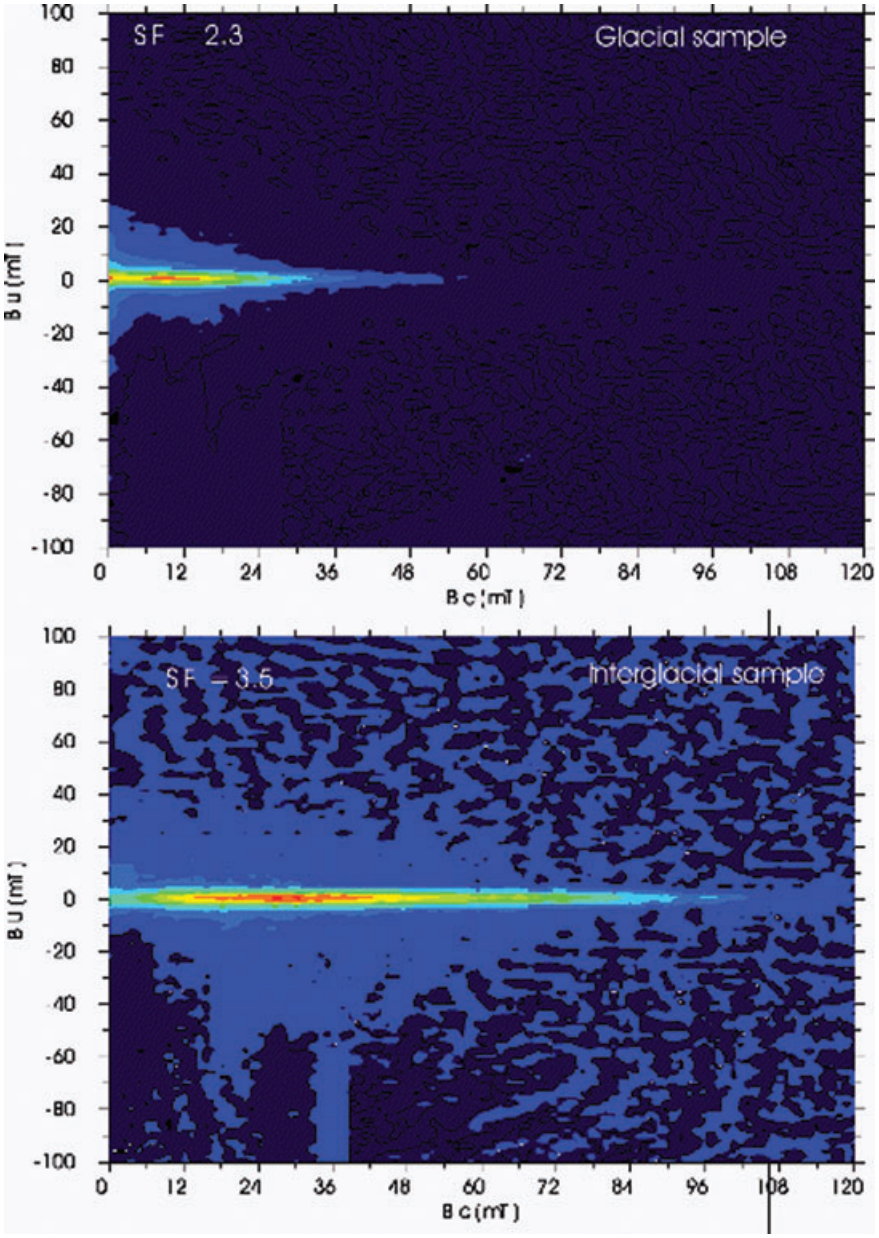

Figure 3. FORC diagrams of the (a) glacial and (b) interglacial samples.

particles. This leads to a second, very low field density maximum centred on Bu and Bc = 0, indicative of particles with a very low or 'zero' coercivity, for example, SP particles (Roberts *et al.* 2000; Pike *et al.* 2001). The identification of SP particles in these samples is perfectly in line with Itambi *et al.* (2009) who measured values of up to 16 per cent for the frequency dependence of susceptibility at extreme glacial events and <4 per cent at interglacial periods.

In the interglacial samples, the FORC distributions display (Fig. 3b) elongated contours that go up to high coercivities close to 90 mT. The lack of visualization of goethite can be attributed to the maximum field of 2 T in which the FORCs were generated.

3.1.3 *Low-temperature results*

Zero-field-cooled and field-cooled warming curves. On warming, the remanences of both samples show a drastic drop between 5 and 25 K, with ∼50 per cent of the remanence lost at 30 K (Figs 4a and b). The remanence decay is stronger in the glacial sample, with over half of the remanence lost before 30 K (Fig. 4a) while only about one-third is lost in the interglacial sample (Fig. 4b). Several reasons have been put forward as an explanation. It may be attributed to the presence of an ultrafine-grained SP phase, which has very low unblocking temperatures. The magnetic disordering of paramagnetic iron bearing minerals that are magnetically ordered at low temperatures has also been related to the rapid drop during this low temperature range (Coey 1988; France & Oldfield 2000). Furthermore, the presence of the magnetic iron sulphide pyrrhotite, which shows a magnetic transition temperature between 30 and 40 K that can be used for its identification (Dekkers *et al.* 1989; Rochette *et al.* 1990) cannot be ruled out as the cause for the decay. The same applies to siderite, which has a Néel temperature of 38 K (Jacobs 1963; Frederichs *et al.* 2003). In addition, potential coatings on and spin glass freezing affect the low temperature signal below 50 K.

From about 30 K upwards, the remanence of the glacial sample (Fig. 4a) gradually decays steadily to minima at room temperature, with only 4 per cent of the initial remanence generated at 5 K retained. In the interglacial sample however (Fig. 4b), a second notable decrease occurs at ∼110 K, interpreted as the Verwey transition of magnetite. This represents a first-order crystallographic phase transition from an inverse cubic spinel to a monoclinic structure, and occurs in stoichiometric magnetite at 117 K (Verwey 1939). The shifted Verwey transition to lower temperatures can result from non-stoichiometric magnetite, for example, partially oxidized magnetite (e.g. Özdemir *et al.* 1993; Dunlop & Özdemir 1997; Smirnov & Tarduno 2000). Also, substitution of Ti for Fe lowers the Verwey transition temperature (e.g. Kakol *et al.* 1992; Moskowitz *et al.* 1998).

AC susceptibility. The behaviour of the susceptibility at low temperature and its frequency dependence is illustrated in Fig. 5. There is a notable difference between interglacial and glacial samples. At glacial intervals, sediments show both temperature and frequency dependence (Fig. 5a). Upon cooling from room temperature (300 K), the susceptibility gently decreases to about 200 K where it begins a gradual increase. This increase culminates in a small broad peak between 130 and 110 K. From ∼100 K, the susceptibility rises sharply, peaking at 50 K. From the maximum peak between 50 and 40 K, the susceptibility drops rapidly to a minimum at 20 K. It

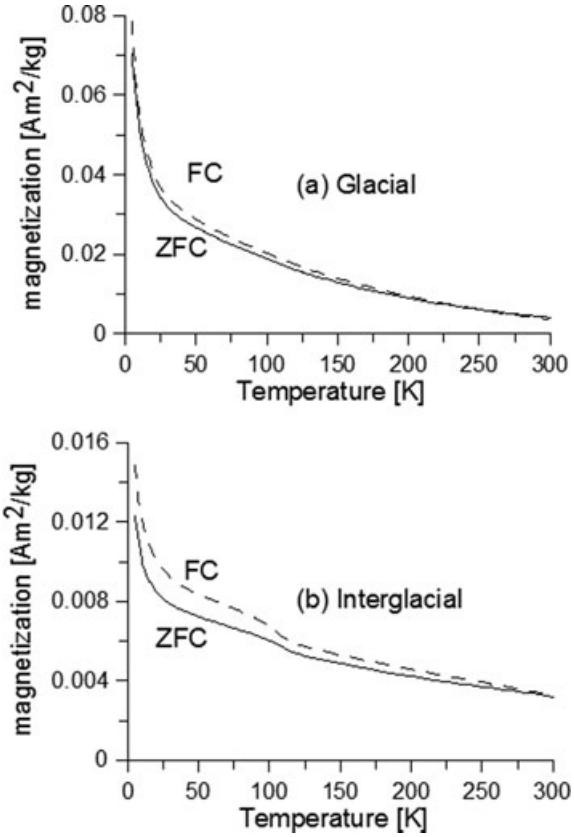

Figure 4. Zero-field-cooled (ZFC) and field-cooled (FC) warming curves of (a) glacial and (b) interglacial sediments between 5 and 300 K. Both show a sharp drop in remanence below ∼30 K.

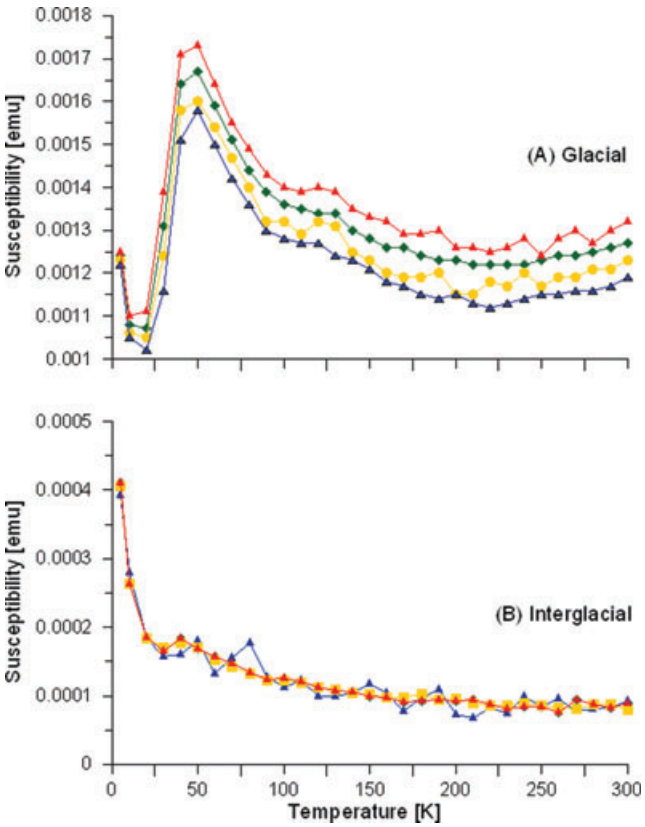

Figure 5. Temperature and frequency dependence of in-phase AC susceptibility between 5 and 300 K.

again begins to rise sharply at 10 K. From the four frequencies, the susceptibility values are highest at the lowest frequency (1 Hz).

The interglacial sediments (Fig. 5b) show just the inverse temperature dependence characteristic of a dominant paramagnetic behaviour as anticipated. AC susceptibility is highest at lowest temperature (5 K) and drops sharply to ∼25 K, after which the rate of decay levels off with increasing temperature. It is approximately constant between 120 and 300 K.

3.1.4 High-temperature magnetic measurements

The two representative bulk samples show distinct signatures during high-temperature cycling of magnetization (Fig. 6). On heating from 25 to 700 °C, the glacial sample (inset in Fig. 6a) shows a continuous, gentle drop in magnetization up to about 500 °C where a change to a steeper slope is observed to ∼600 °C. Above this temperature, it remains fairly constant although there is a tiny drop at ∼670 °C, a minute hint to the presence of haematite. The cooling curve is reversible up to 680 °C (because this part is paramagnetic) and then steadily increases though with a smaller magnetization compared to the initial heating curve.

The interglacial sample shows a markedly different response during heating (inset in Fig. 6b). The curve shows a gentle decrease in magnetization from room temperature up to 360 °C where it rises abruptly to values close to the starting magnetization value. This increase in the magnetization maintains a broad peak between 420 and 475 °C that slightly dips towards higher temperatures, culminating in a sharp drop between 475 and ∼600 °C. From 600 to 700 °C, the drop is gentle, consistent with that observed at temperatures <360 °C. The cooling curve is non-reversible and has a magnetization lower than that of the heating curve. The observed jump at 360 °C is consistent with high-temperature oxidation of non-magnetic iron phases into magnetic phases (e.g. Passier *et al.* 2001). Oxidation progresses via magnetite, maghemite, to haematite. The broadness of the oxidation peak in the present sediments shows that the two different types of pyrite (i.e. framboids and euhedral pyrite) jointly occur as will be seen in the SEM pictures (Section 3.2.3). The non-magnetic Fe-bearing clay mineral nontronite was identified from X-ray diffraction analysis (data not shown). Thermal treatment of nontronite (Moskowitz & Hargraves 1984) reveals that paramagnetic behaviour persists during heating above 700 °C which rules out its contribution to the thermal behaviour of our sample.

To document the alteration in greater detail we also performed so-called incremental thermomagnetic runs (Figs 6c and d). They show indeed the alteration and the occurrence of minute amounts of pyrite in the glacial sample. Its presence could only be vaguely surmized from the single segment thermomagnetic run. It is evident that the magnetite formed oxidizes rapidly to haematite (the magnetization tail at temperatures to 600–620 °C is barely noticeable). Importantly, in both glacial and interglacial samples there is a small decrease in magnetization from 250 °C upwards. This could be due to the presence of maghemitized coatings on magnetite particles (glacial samples) or possibly due to the presence of intermediate monosulphides (primarily greigite) that are chemically removed at that temperature range (interglacial samples).

3.2 Scanning electron microscopy

SEM analysis was performed on magnetic extracts and HLS. A wide range of iron-bearing mineral phases were observed with a significant distinction between glacial and interglacial sediments. The iron oxides and sulphides of prime interest here, include pure iron oxides, titanium bearing iron oxides and iron sulphides. The particles occur in a broad grain-size range, varying from a few hundreds of nanometres to tens of microns, reflecting the complex sedimentary environment with various sources of the magnetic assemblage.

3.2.1 Iron oxides

Pure iron oxides constitute a large fraction of the extracts, that is, approximately 30 per cent in the glacial sample and ∼20 per cent at the interglacial stage. They vary both in size and shape, with the dominant shapes being spherules and irregular shaped grains. A greater proportion of the iron oxides are made up of irregularly shaped rounded grains ranging in size from a few micrometres to ∼30 μm.

Magnetic spherules with different surface features, comprising well-rounded, smooth as well as rough exteriors were observed (Fig. 7). The general composition includes pure iron oxides to iron oxides with Al and Si inclusions, as well as Fe-Ti oxides. Spherules deposited during interglacials were fewer in number, smoother and entirely composed of Fe and O (Fig. 7f).

Spherules shown in Figs 7(a) and (b) are composed of Fe and O with small inclusions of Al and Si as was observed from the EDS. We classify these as magnetite spherules based on previous studies that have identified similar particles (Freeman 1986: Suk *et al.* 1990; Sun & Jackson 1994; Franke *et al.* 2007b).

Fig. 7(d) shows a broken spherule demonstrating its internal framework while Fig. 7(e) is a chunk of some of the building blocks that has disintegrated from a broken spherule. The internal

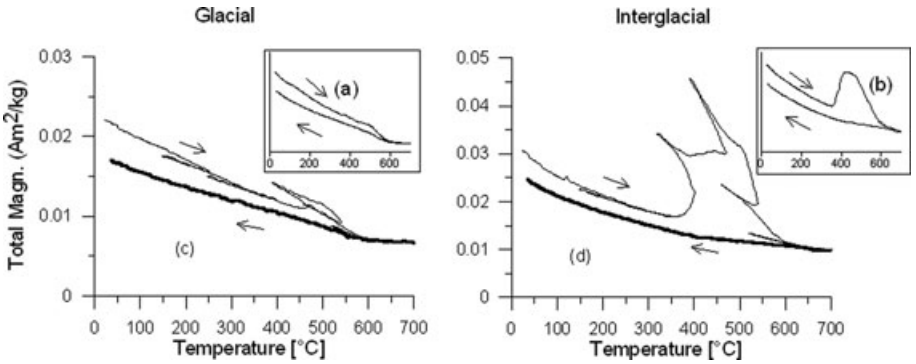

Figure 6. Thermomagnetic runs measured on a translation type Curie balance in air. The insets are single runs from room temperature to 700 °C and back. The other two curves are incremental runs performed to detect potential thermal transformations. Incremental runs were performed at maximum temperatures of 250, 350, 400, 470, 540, 620 and 700 °C.

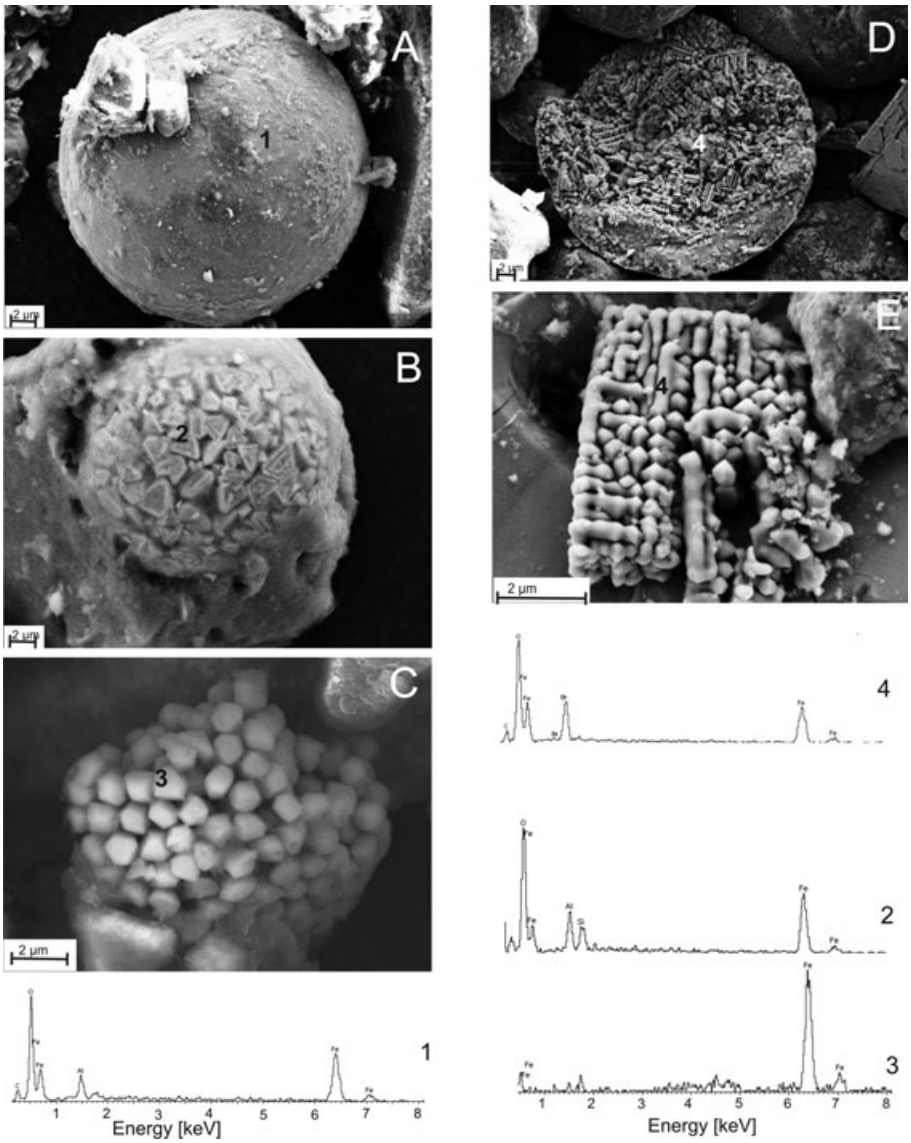

Figure 7. SEM micrographs of iron oxides obtained in secondary electron (SE) mode. The numbers on the micrographs indicate the position where EDS spectra (shown with identical numbering) were obtained. (a) Spherule with smooth surface. (b) Magnetic spherule with interlocking triangular crystals. (c) Magnetite framboids of biogenic origin. (d) The internal framework of a split spherule, displaying dendritic structures. (e) A further display of some of the building blocks of the spherule.

morphology shows well-developed dendritic structures, which indicate rapid crystallization from a high-temperature melt. Fe, O and Br are the three chemical components identified with EDS. The 'Br' cannot occur in large amounts, so the line is actually the L line of Al, which has the same energy position as the K line of Br.

The partially disintegrated framboid in Fig. 7(c) is composed of small euhedral particles measuring ∼600 nm in a very regular array. In some EDS spectra only Fe was detected and in others both Fe and O. Although no traces of sulphur were identified, the morphology and arrangement of the microcrystals point towards a biogenic origin. McCabe *et al.* (1987) and Suk *et al.* (1990) among others have reported the occurrence of such oxidized framboids and classify them as of secondary origin formed by the transformation of framboidal pyrite. Such framboids could consist of diagenetic magnetite formed by the oxidation of pyrite.

Magnetic spherules in marine environments may originate from a number of sources, that is, cosmic, diagenetic, anthropogenic and volcanic sources, each with distinctive characteristics. The presence of nickel is a strong indicator for cosmic origin (Fredriksson & Martin 1963; El Goresy 1968; Parkin *et al.* 1980). None of the identified grains showed traces of Ni. However, Ni is readily depleted in the crust of the spherules during ablation processes during passage through the Earth's atmosphere. This implies that only analysis of a broken or cut (and polished) particle or thin section can provide a genuine conclusion about its origin. This shows an iron oxide-rich composition without Ni. This evidence rules out a cosmic origin for the particles. Sediments are obviously too old for an anthropogenic origin. Spherules of diagenetic origin produced from framboidal pyrite oxidation (Suk *et al.* 1990) occur and are easy to identify because of their characteristic shape (Fig. 7c).

The presence of Ti is diagnostic of volcanic spherules (Fredriksson & Martin 1963; Freeman 1986; Franke *et al.* 2007b). The broken spherule observed in our sediments made it possible to measure the internal composition. The lack of an interlocking crystal surface and imperfect spherical forms are attributed to a volcanic origin. The interlocking triangular crystals observed in Fig. 7(b)

might suggest an extraterrestrial source. However, the presence of Al and Si in its spectra rules out this source.

3.2.2 Fe-Ti oxides

About 60 per cent of the magnetic particles in the glacial sample and 25 per cent in the interglacial sample consist of Ti-bearing iron oxides. The degree of substitution varies significantly, with some grains containing more Ti than Fe. Their shapes and grain sizes also vary, with typical size range of between 1 and 30 μm. Most of the grains are irregularly shaped with rounded features.

The Ti-bearing particles in the glacial samples (Figs 8a–d) show a wide range of features prominent among which are the titanohaematite lamellae intergrown with titanomagnetite (TM,

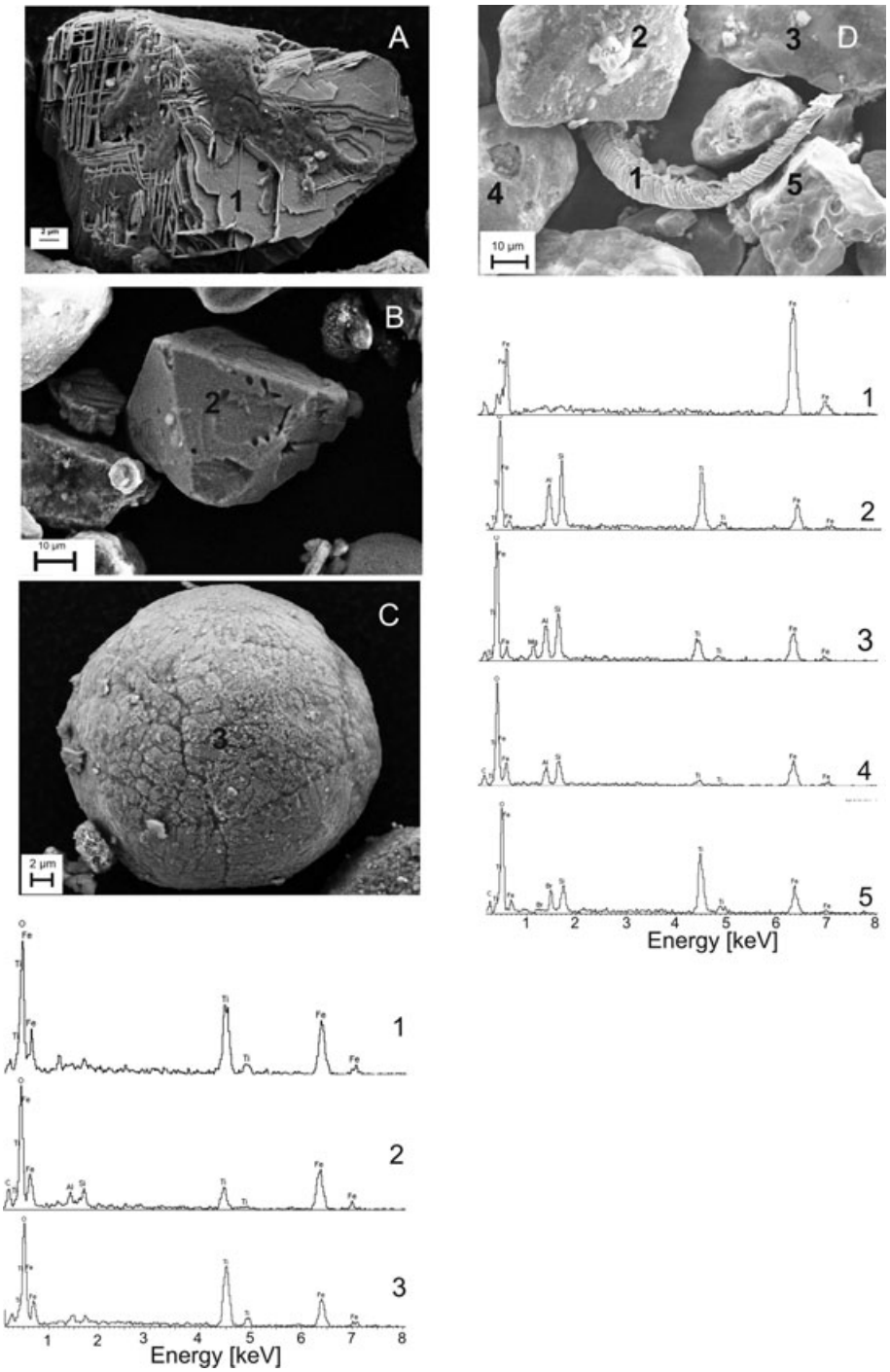

Figure 8. SEM micrographs of iron-titanium oxides obtained in secondary electron (SE) mode. The numbers on the micographs indicate position where EDS spectra (shown with identical numbering) were obtained. (a) Haemoilmenite grain displaying ilmenite lamellae after the titanohaematite intergrowths have been preferentially dissolved. (b) Octahedral titanomagnetite grain with sharp edges, displaying dissolution marks and surrounded by irregularly shaped titanomagnetite grains and spherule. (c) Titanium-rich spherule of possible volcanic origin with mild dissolution features. (d) Amorphous grains with an unidentified magnetic structure of possibly organic origin.

Fig. 8a). Freeman (1986), von Dobeneck *et al.* (1987), Garming *et al.* (2005, 2007) and several others have described such intergrowths to be products of high-temperature oxidation of TM. Fig. 8(a) which shows exsolution textures of the Fe-Ti-oxide intergrowth with preferential dissolution of the TM intergrowth that left behind the more resistant titanohaematite or ilmenite lamellae. Freeman (1986) used the exsolution features of such minerals and the Ti content to suggest a basic magma source. The shrinkage cracks observed indicates low-temperature oxidation (Petersen & Vali 1987). Fig. 8(b) shows an octahedral TM particle with sharp edges and dissolution marks which suggest possible aeolian transport. The inclusion of Ti and the large grain size rules out biomineralization as a source.

Fig. 8(c) shows a Ti-rich spherule with a rough surface morphology that may be attributed to dissolution (Franke *et al.* 2007b). Fig. 8(d) shows irregularly shaped Fe-Ti-O particles with some indicating dissolution. Also identified is an Fe-O-rich structure of possibly organic origin. Interglacial samples with typical grain sizes ranging between 1 and 10 μm showed lower concentration of Fe-Ti-O, with strong dissolution features.

3.2.3 Iron sulphides

Although iron sulphides were previously believed to be of little significance to the magnetic properties, recent studies have emphasized their relevance to palaeomagnetism, post-depositional and environmental reconstruction. Indeed, we document their occurrence also in our samples. The iron sulphides were observed in the heavy fraction extracted by HLS and not by the magnetic extraction. This implies a non-magnetic iron sulphide, (almost) all pyrite when expressed on a molar basis. The occurrence of iron sulphides in glacial sediment was very limited, making up less than 2 per cent of the extract. The presence of a minute quantity of pyrite was also revealed by the thermomagnetic analysis (Fig. 6a).

Typical micrographs of the iron sulphides are illustrated in Figs 9(a) and (b). They are the dominant Fe-bearing minerals in interglacial sediments, making up over 50 per cent of the iron-bearing component. They occur as framboids with a fairly wide range of sizes (between 6 to 14 μm), the framboids consist of euhedral microcrystals measuring between 0.1 and 1 μm in diameter with different crystal shapes. Framboids also occur in large clusters which can reach dimensions of ∼250 × 480 μm (Fig. 9a). The octahedron and truncated octahedron shapes depicted in Fig. 9(b) strongly suggest a biogenic origin.

A cluster of irregularly shaped magnetic grains composed of iron and oxygen (EDS), which was uncovered from the glacial sample (Fig. 10). Based on its composition it could be interpreted as oxidized pyrrhotite. Freeman (1986) reported a similar grain cluster of iron and sulphur composition which he classified as pyrrhotite crystals held together by magnetic attraction.

Pyrrhotite can be formed diagenetically under very reducing conditions with abundant pyrite. However, it has been shown (Schoonen & Barnes 1991; Lennie *et al.* 1995) that low temperatures do not favour pyrrhotite formation. Metamorphic rocks are potential sources of detrital pyrrhotite in sediments (Horng & Roberts 2006). Such rock types constitute the source for sediments transported from the African continent to the continental margin.

4 DISCUSSIONS

Low- and high-temperature experiments, FORC analysis and SEM observations provide diagnostic features that can be used to identify and characterize the magnetic mineral content of these sediments. Here we put all information into a larger palaeoenvironmental, palaeoclimatic and diagenetic context.

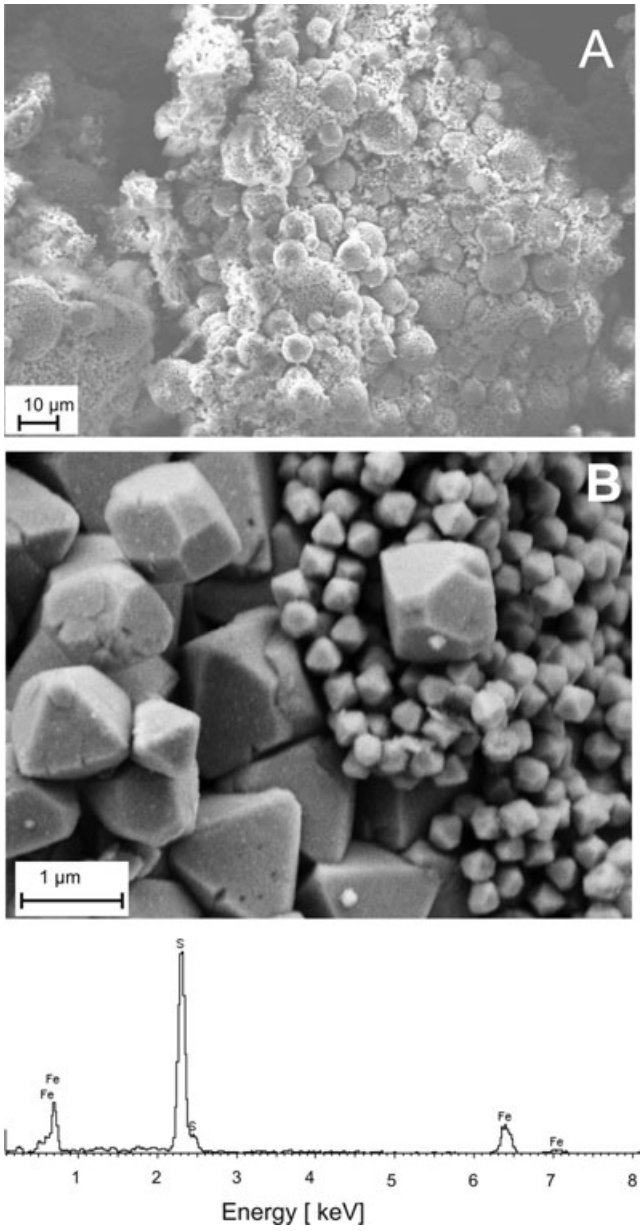

Figure 9. Typical SEM micrographs of iron sulphides obtained in secondary electron (SE) mode. The numbers on the micographs indicate position where EDS spectra (shown with identical numbering) were obtained. (a) Cluster of numerous pyrite framboids of different sizes. (b) Two sizes of euhedral pyrite microcrystals. Note also the crystal shapes (octahedron and truncated octahedron).

4.1 Magnetic interpretation

IRM component analysis (Table 1 and Fig. 2) shows that the magnetic properties of our sediment samples are mostly dominated by magnetite, haematite and goethite. The degree of influence of each mineral varies with respect to glacial and interglacial stages. Magnetite is the most dominant component at both stages, with a distinctively higher concentration at interglacials. High haematite

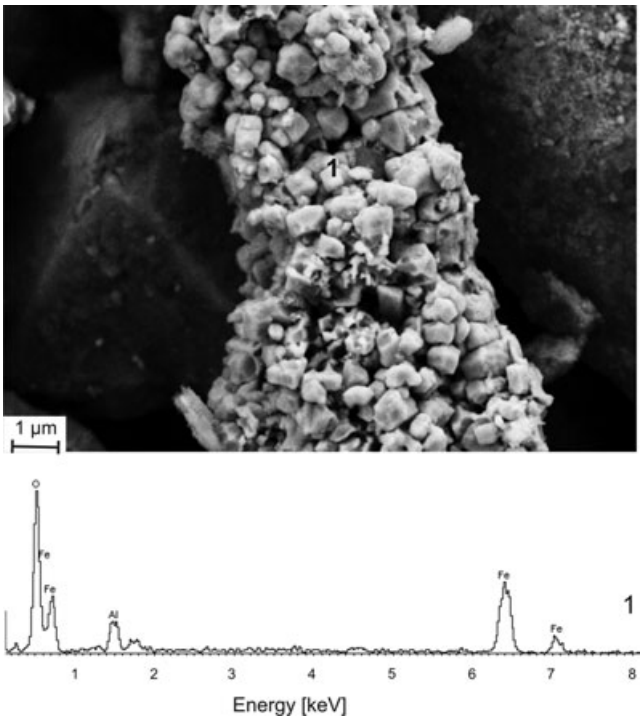

Figure 10. SEM micrographs of oxidized pyrrhotite obtained in secondary electron (SE) mode.

and goethite on the other hand, exert more influence at glacials as shown in Table 1 and Fig. 2.

Magnetite presence is also confirmed by the identification of the Verwey transition in the interglacial samples at ∼110 K. This transition however is absent in the glacial sample where magnetite contribution is significantly less. Non-stoichiometry, cation substitution and grain size have been attributed to the suppression and disappearance of the Verwey transition (Syono 1965; Kakol & Honig 1989; Kakol *et al.* 1992; Halgedahl & Jarrard 1995). There is enough evidence in our samples to suggest that all three factors may have contributed in the masking of the transition at glacial intervals. The higher DP of magnetite in the IRM component analysis of these samples is interpreted as evidence for the partial oxidation of magnetite. The softer IRM component in the interglacial sample may be related to a core-shell situation whereby, mild reduction dissolves the shell of the particles leading to reduction of the DP and making the Verwey transition observable. This results in the skewing of the coercivity distribution to the left as observed in IRM acquisition curve. Ti-rich TM were among the dominant minerals identified from EDS. Moskowitz *et al.* (1998), demonstrated the effects of Ti substitution on the low-temperature characteristics of magnetite. They observed that the transition temperature T_v decreases with increasing Ti substitution. For TM ($Fe_{3-x}Ti_xO_4$) with $0 < x < 1$, it has been shown (Kakol *et al.* 1992) that the Verwey transition is suppressed for $x > 0.04$. Since EDS is semi-quantitative, we cannot determine a precise value for x in our samples. However, the high percentage of Ti identified in the titanomagnetite suggests x to be abundant enough to have led the suppression. SP particles identified with FORCs diagrams and susceptibility also contributed to the masking of the Verwey transition.

Goethite was detected as the dominant high-coercivity mineral, contributing about 42 per cent of the remanence in glacial samples and about 8 per cent in the interglacial samples. A haematite fraction was also identified but in significantly smaller amounts, that is, 8 per cent during glacial and about 5 per cent at interglacial. Although Itambi *et al.* (2009) observed strong evidence for the presence of haematite and goethite in these sediments, no low-temperature transitions were observed to support these results. However, the lack of the Morin transition (T_m) does not only imply the absence of haematite since the degree of stoichiometry and particle grain sizes are known to affect this transition. Morin (1950) showed that T_m can be completely suppressed with the addition of ∼1 per cent Ti to the crystal lattice. Small particle sizes of less than 30 nm have also been reported (Bando *et al.* 1965; Özdemir *et al.* 2008) to suppress T_m. Haematite and goethite have been suggested to occur as ultrafine coatings on quartz grains from the Saharan desert deposited in the Atlantic Ocean (Balsam *et al.* 1995). Although the HLS method enabled all the iron phases to be extracted from the bulk sediment, the limitation in the resolution of SEM hindered the identification of ultrafine particles.

Goethite is formed under humid climate (Schwertmann *et al.* 1985; Schwertmann 1988; Cornell & Schwertmann 1996), and therefore is formed in the Sahelian region of West Africa where present day precipitation is received up to 20 °N. The dominance of this mineral over haematite illustrates that the sediments deposited in this region of the Senegal continental margin are derived from the Sahel rather than from the Sahara region. Goethite formed during humid period is eroded and transported to the continental margin during dry period. Reddened desert sands (pigmented by haematite and goethite) have previously been used to trace the distribution of aeolian dust in marine sediments (Diester-Hass 1976; Balsam *et al.* 1995; Itambi *et al.* 2009). Goethite abundance also shows that glacial periods were marked by a southward shift or constriction of the precipitation band (tropical rainbelt), leading to drought in the Sahel. Kalu (1979) and Sarnthein & Koopman (1979) reported these pigmented sediments to originate from the zone of ferrallitic soils south of the Sahara and in the Sahel region, an area that is periodically under the influence of humid conditions.

Low temperature measurements have also provided further evidence for the variation in the magnetic mineralogy. Different reasons have been proposed to explain the rapid decrease in the remanence between 5 and 30 K. These include (1) contributions from SP particles, (2) paramagnetic materials (e.g. silicates) that become ordered at very low temperature and (3) ferromagnetic haemoilmenite. One or more of these factors may possibly contribute to the observed signal in our records. The presence of SP particles in the glacial samples has been confirmed by FORCs measurements and AC susceptibility. The magnetic mineral contributing to this phase is still not yet identified but we suggest haematite and goethite as the probable cause based on the high frequency-dependent susceptibility and its positive correlation to HIRM as illustrated by Itambi *et al.* (2009). Haemoilmenite (Fe_2O_3-$FeTiO_3$) with 8–10 mole per cent of haematite was suggested as a possible low-temperature SP phase in subaerial basalts (Kosterov 2001). This solid solution series was identified using SEM in our glacial sediments. Despite the fact that the interglacial samples showed no presence of SP particles and haemoilmenite, their remanences also responded in a similar pattern below 30 K as reflected in the ZFC and FC curves. This can be attributed to paramagnetic clay minerals contained in both samples and derived from the African continent via aeolian and fluvial pathways. The clay particles are paramagnetic at room temperature and at very low temperatures become magnetically ordered (Coey 1988).

The AC susceptibility curve between 5 and 100 K is similar to that obtained for TM bearing samples of basaltic material from the Hawaiian deep drill hole (SOH1) (Moskowitz *et al.*

1998) and haemoilmenite solid solution series (Gehring *et al.* 2007; Burton *et al.* 2008). Moskowitz *et al.* (1998) suggested that their observations may be as a consequence of the superposition of paramagnetic, anti-ferromagnetic and ferromagnetic susceptibilities from different iron phases. It is also reasonable to consider that our record reflects these different properties exhibited by different iron-bearing phases including an ilmenite-dominated haemoilmenite solid solution and TM. These are evident from SEM observations of our glacial sediments. In the susceptibility versus temperature curves, the peak occurring at ∼50 K represents the Néel temperature of ilmenite, which deviates from the 56 K value for pure ilmenite due to dilution by haematite in the solid solution series (Kato *et al.* 1982). Judging from the similarity of our record to that of Burton *et al.* (2008), we suggest $X = \sim 0.6$ in the haemoilmenite solid solution $[(1–X)Fe_2O_3–(X)FeTiO_3]$. The subsequent sharp drop in susceptibility after 40 K on cooling indicates spin glass freezing where the system transforms from a magnetically ordered phase to a disordered low-temperature glassy phase.

4.2 Diagenetic sulphidization

High-temperature magnetic measurements show that non-magnetic iron phases are dominant in our samples. This is clearly the case in the interglacial sample where the sediment undergoes thermal transformation at 360 °C, which is consistent with the high-temperature oxidation of a non-magnetic iron phase into a magnetic phase.

This thermomagnetic behaviour is virtually the same as that observed for sapropel S1 in Mediterranean sediments by Passier *et al.* (2001). They identified two types of pyrites through their high-temperature oxidation behaviour. They reported that framboidal pyrite aggregates of 5–10 μm size range (with individual framboids submicron in size) were easily oxidized at lower temperatures starting at ∼360 °C because of their large reactive surface area. Euhedral pyrite on the other hand was oxidized at temperatures starting at ∼420 °C. The broadness of the oxidation peak in our samples shows that the two types of pyrite (i.e. framboids and euhedral pyrite) jointly occur in our interglacial sediments. The scanning electron micrographs of the magnetic extracts clearly support the evidence for this joint occurrence, with both euhedral and framboidal pyrite identified.

Reductive dissolution of magnetic particles in sediments has been widely documented (e.g. Canfield & Berner 1987; Karlin 1990) and may result in the loss of the primary natural remanent magnetization signal via the formation of new iron phases. Sulphidization has been used to reconstruct past environmental conditions at a depositional site (e.g. Hawthorne & Mckenzie 1993). High productivity and availability of organic matter provides a thriving environment for microphylic bacteria, which produces H_2S (Froelich *et al.* 1979) that reacts with dissolved ferrous iron, forming greigite. In the presence of high sulphide concentration, the greigite further reacts to produce the more stable pyrite (Sweeney & Kaplan 1973; Berner 1984). Several formation pathways for pyrite framboids have been proposed, but none seems to be generally accepted. Some authors (Sweeney & Kaplan 1973; Wilkin & Barnes 1997) have suggested greigite as a pre-requisite for framboid formation whereas more recent studies (Butler & Rickard 2000) dispute such claims, demonstrating that framboids could be formed by the oxidation of ferrous iron monosulphide by hydrogen sulphide. Taylor (1982) showed that framboid formation could take place in free suspension by the coagulation of iron sulphide gel particles which, in a marine environment, could be the result of biogenic bisulphide ions reacting with Fe^{2+}. Framboid formation is rapid, emanating from aqueous solutions highly saturated with iron monosulphide and pyrite. Euhedral textures on the other hand form slowly in less saturated environments (Sweeney & Kaplan 1973; Goldhaber & Kaplan 1974).

Low concentrations (<2 per cent) of euhedral pyrite in our glacial sediments therefore suggest minimal diagenesis. The presence of both framboidal and euhedral pyrite at the interglacial suggests that secondary pyrite formation continued at slow rates after burial, yielding euhedral particles. This resulted because most of the reactive iron had been reduced during early diagenesis and sulphate reduction rates were much lower comparable to recently deposited organic matter (Passier *et al.* 1999). This therefore suggests that strong anoxic bottom water conditions existed during warmer periods at our study location.

4.3 Diagenesis and dissolution

Although the previous section documents evidence for diagenesis, this was however not identified at this location by Itambi *et al.* (2009) using the reductive diagenesis proxy $Fe/\kappa_{nd,}$ (where κ_{nd} is the non-diamagnetic susceptibility), (Funk *et al.* 2004). The anhysteretic remanent magnetization and IRM intensities were also high as compared to the other cores (GeoB 9506–1 and GeoB 9527–5) that showed evidence of dissolution. A probable explanation for such discrepancy is that, here, we are dealing with multiple sources of Fe. The Fe/κ_{nd} parameter (Funk *et al.* 2004) is mostly suitable for diagenesis investigations where there is a single source that operates to a variable degree. The Senegal and Gambia Rivers have been documented as pathways through which a significant amount of dissolved Fe and suspended particles are transported to this location (Gac & Kane 1986a, b). Some of the dissolved iron is precipitated at the mixing zone between fresh and sea water, producing magnetic phases such as goethite (Odin 1975). These secondary minerals and dissolved Fe in the pore water may provide reactive substances for later reaction with sulphide. In this scenario, the detrital magnetic particles will remain unaffected by dissolution provided there is sufficient reactive iron available. In the Arabian Sea, reductive diagenesis has been credited with the preservation of the primary signals (deMenocal *et al.* 1991). Fine-grained magnetite produced *in situ* by magnetotactic bacteria are preferentially dissolved during oxidation of organic matter, whereas the primary magnetic particles that represent climate variations remain (largely) unaffected.

Our records show evidence consistent with the dissolution of magnetic minerals that follow a systematic glacial/interglacial climatic pattern. All the glacial intervals studied indicated little or no evidence of reductive diagenesis, whereas the interglacials were heavily affected, evident from the high concentration of pyrite framboids. Climatically driven changes in marine productivity and grain-size variation could have resulted in the observed signals. Hawthorne & Mckenzie (1993), have shown in lacustrine environment of Lake Greifen that productivity-modulated redox conditions of the sedimentary environment impact the magnetic properties.

Marine productivity in the Senegal region is stimulated also during glacial periods by enhanced upwelling driven by stronger NE trade winds but these samples show minimal diagenesis. Organic matter produced in the marine environment is therefore not responsible for the anoxic conditions that may have persisted during interglacials. Organic matter of terrigenous origin transported via rivers was of great significance in fostering dissolution of magnetic particles. Warmer conditions at these periods are usually characterized by enhanced precipitation that penetrates further north on

the northwest African continent, leading to vegetation cover in the Sahel region. The increase in precipitation, vegetation cover and drainage intensity facilitates the influx of terrestrial organic matter into the ocean. Bird *et al.* (1998) illustrated the seasonal dependence of organic matter in a river (River Sanaga in Cameroon), attributing higher concentrations to periods of high river discharge (wet season) and low concentration to low discharge (dry season).

Smaller grain sizes of the magnetic particles during interglacials might have also contributed to the significant dissolution of the minerals. Several authors (e.g. deMenocal *et al.* 1991; Bloemendal *et al.* 1993) have shown the preferential dissolution of fine-grained magnetic minerals in sediments. As observed in our records, the glacial sediments are much coarser, with the magnetic particles sizes ranging between 1 and 30 μm whereas the finer interglacial cycles are dominantly <10 μm. Our results are consistent with previous studies that have classified the grain size of silt deposited in the west African continental margin, and originating from the Sahara/Sahel region to be larger at glacials (>10 μm), and finer at interglacial (<10 μm and mostly transported by rivers) (Sarnthein *et al.* 1981; Rognon *et al.* 1996; Stuut *et al.* 2005).

5 CONCLUSIONS

The characterization of the magnetic mineral assemblages reveals that the Senegal continental margin is a complex sedimentary setting in terms of magnetic mineralogy. Detrital magnetic mineral fluxes tend to be controlled by fluvial and aeolian transport pathways, which are modulated by shifts between humid and arid climate over northwest Africa. Larger grain sizes observed for the glacial sediments together with higher goethite and haematite contributions reflect stronger wind strengths and aridity over northwest Africa and the Sahel in particular. In contrast, interglacials are dominated by finer magnetic particles, which is a reflection of fluvial transport resulting from intense precipitation.

Identification of pyrite by both thermomagnetic analysis and SEM suggests that both framboidal and euhedral pyrite dominate the iron-bearing phases at interglacial intervals. Pyrite dominance is evidence for the post-depositional alteration of the magnetic minerals. The occurrence at all interglacial intervals studied (only one shown here) suggest that diagenesis was climate driven, possibly stimulated by the finer magnetic particles and terrestrial organic matter input.

The occurrence of secondary magnetite points to a remagnetization of these sediments, imparting a chemical remanence that might mask the primary signals (Suk *et al.* 1990; Sun & Jackson 1994; Rowan & Roberts 2006). However the degree to which this secondary magnetization has affected the primary signal over northwest Africa is minimal as very few of such particles were observed. This is also true for non-climate-related magnetic spherules that also occur in the sediments in low concentration.

ACKNOWLEDGMENTS

We thank Petra Witte for her support with the electron microscopy and the members of the Paleomagnetic Laboratory at Utrecht University (where part of this work was done) for their support. We also acknowledge Christine Franke for performing some of the Curie balance measurements and providing helpful suggestions. This work was supported by the German Research Foundation (DFG) through the European graduate college EUROPROX (University of Bremen).

REFERENCES

Balsam, W.L., Otto-Bliesner, B.L. & Deaton, B.C., 1995. Modern and last glacial maximum aeolian sedimentation patterns in the Atlantic Ocean interpreted from sediment iron oxide content, *Paleoceanography,* **10,** 493–507.

Bando, Y., Kiyama, M., Yamamoto, N., Takada, T., Shinjo, T. & Takaki, H., 1965. The magnetic properties of γ-Fe_2O_3 fine particles, *J. Phys. Soc. Japan,* **20,** 2086.

Berner, 1984. Sedimentary pyrite formation: an update. *Geochim. cosmochim. Acta.,* **48,** 605–615.

Bird, M.I., Giresse, P. & Ngos, S., 1998. A seasonal cycle in the carbon-isotope composition of organic carbon in the Sanaga river catchment, Cameroon, *Limnol. Oceanograph.,* **43,** 111–114.

Bloemendal, J., Lamb, B. & King, J., 1988. Paleoenvironmental implications of rock-magnetic properties of late Quaternary sediment cores from the eastern Equatorial Atlantic, *Paleoceanography,* **3,** 61–87.

Bloemendal, J., King, J.W., Hunt, A., deMenocal, P.B. & Hayashida, A., 1993. Origin of the sedimentary magnetic record at Ocean Drilling Program Sites on the Owen Ridge, western Arabian Sea, *J. geophys. Res.,* **98,** 4199–4219.

Brownlee, D.E., 1981. Extraterrestrial components, in *The Sea,* Vol. **7**, pp. 733–762, ed. Emiliani, C., John Wiley, New York.

Brownlow, A., Hunter, E.W. & Parkin, D.W., 1966. Cosmic spherules in a Pacific core, *Geophys. J. R. astr. Soc.,* **12,** 1–12.

Burton, B.P., Robinson, P., McEnroe, S.A., Fabian, K. & Ballaran, T.B., 2008. A low-temperature phase diagram for ilmenite-rich compositions in the system Fe_2TO_3–$FeTiO_3$, *Am. Mineral.,* **93,** 1260–1272.

Butler, I.B. & Rickard, D., 2000. Framboidal pyrite formation via the oxidation of iron (II) monosulfide by hydrogen sulfide, *Geochim. cosmochim. Acta.,* **64,** 2665–2672.

Canfield, D.E. & Berner, R.A., 1987. Dissolution and pyritization of magnetite in anoxic marine sediments, *Geochim. cosmochim. Acta.,* **51,** 645–659.

Coey, J.M.D., 1988. Magnetic properties of iron in soil iron oxides and clay fractions, in *Iron in soils and clay minerals,* pp. 397–466, eds Stucki, J.W. *et al*., Reidel, Dordrecht, the Netherlands.

Cornell, R.M. & Schwertmann, U., 1996. *The Iron Oxides: Structure, Properties, Reactions, Occurrence and Uses,* VCH, Weinheim.

Dekkers, M.J., Mattéi, J.L., Fillion, G. & Rochette, P., 1989. Grain size dependence of the magnetic behaviour of pyrrhotite during its low temperature transition at 34 K, *Geophys. Res. Lett.,* **16,** 855–858.

deMenocal, P., Bloemendal, J. & King, J., 1991. Rock magnetic record of monsoonal dust deposition to the Arabian Sea: evidence for a shift in the mode of deposition at 2.4 Ma. Proceed. ODP, *Sci. Results,* **117,** 389–407.

Diester-Haas, L., 1976. Late Quaternary climate variations in North West Africa deduced from East Atlantic sediments cores, *Quat. Res,* **6,** 299–314.

Dunlop, D.J. & Özdemir, Ö., 1997. *Rock Magnetism: Fundamentals and Frontiers. Cambridge Studies in Magnetism,* Cambridge University Press, Cambridge.

Egli, R., 2004. Characterization of individual rock magnetic components by analysis of remanence curves, 1. Unmixing natural sediments, *Stud. Geophys. Geod.,* **48**(2), 391–446.

El Goresy, A., 1968. Electron microprobe analysis and ore microscopic study of magnetic spherules and grains collected from the Greenland Ice, *Beitr. Min. und Petr*., **17,** 331–346.

France, D.E. & Oldfield, F., 2000. Identifying goethite and hematite from rock magnetic measurements of soils and sediments, *J. geophys. Res.,* **105,** 2781–2799.

Franke, C., Frederichs, T. & Dekkers, M.J., 2007a. Efficiency of heavy liquid separation to concentrate magnetic particles, *Geophys. J. Int.,* **170,** 1053–1066.

Franke, C., von Dobeneck, T., Drury, M.R., Meeldijk, J.D. & Dekkers, M.J., 2007b. Magnetic petrology of equatorial atlantic sediments: electron microscopic results and their environmental magnetic implications, *Paleoceanography,* **22,** 4207, doi:10.1012/2007PA001442.

Frederichs, T., von Dobeneck, T., Bleil, U. & Dekkers, M.J., 2003. Towards the identification of siderite, rhodochrosite, and vivianite in sediments by their low-temperature magnetic properties, *Phys. Chem. Earth,* **28,** 669–679.

Fredriksson, K. & Martin, L.R., 1963. The origin of black spherules found in the Pacific islands, deep-sea sediments, and Antarctic ice, *Geochim. cosmochim. Acta.,* **27,** 245–248.

Freeman, R., 1986. Magnetic mineralogy of pelagic limestones, *Geophys. J. R. astr. Soc.,* **85,** 433–452.

Froelich, P.N. *et al*., 1979. Early oxidation of organic matter in pelagic sediments of the eastern equatorial Atlantic: suboxic diagenesis, *Geochim. cosmochim Acta.,* **43,** 1075–1090.

Funk, J. A., von Dobeneck, T. & Reitz, A., 2004. Integrated rock magnetic and geochemical quantification of redoxomorphic iron mineral diagenesis in late quaternary sediments from the equatorial Atlantic, in *The South Atlantic in the Late Quaternary: Reconstruction of Material Budget and Current Systems,* pp. 237–260, eds Wefer, G., Mulitza, S. & Ratmeyer, V., Springer-Verlag, Berlin.

Gac, J.Y. & Kane, A., 1986a. Le fleuve Sénégal. I- Bilan hydrologique et flux continentaux de matières particulaires à l'embouchure, *Sci. Geol. Bull.,* **39,** 99–130.

Gac, J.Y. & Kane, A., 1986b. Le fleuve Sénégal II- Flux continentaux de matières dissoutes a l'embouchure, *Sci. Geol. Bull.,* **39,** 151–172.

Garming, J.F.L., Bleil, U. & Riedinger, N., 2005. Alteration of magnetic mineralogy at the sulfate methane transition: analysis of sediments from the argentine continental slope, *Phys. Earth planet. Inter.,* **151,** 290–308.

Garming, J.F.L., Bleil, U., Franke, C. & von Dobeneck, T., 2007. Low-temperature partial magnetic self-reversal in marine sediments by magnetostatic interaction of titanomagnetite and titanohematite intergrowths, *Geophys. J. Int.,* **170**(3), 1067–1075.

Gehring, A.U., Fischer, H., Schill, E., Granwehr, J. & Luster, J., 2007. The dynamics of magnetic ordering in a hemo-ilmenite solid solution, *Geophys. J. Int.,* **169,** 117–125.

Goldhaber, M.B. & Kaplan, I.R., 1974. The sulfur cycle, in *The Sea,* Vol. **5**, pp. 569–655, Wiley, New York.

Halgedahl, S. & Jarrard, R.D., 1995. Low-temperature behavior of single-domain through multidomain magnetite, *Earth planet. Sci. Lett.,* **130,** 127–139.

Harrison, R.J. & Feinberg, J.M., 2008., FORCinel: an improved algorithm for calculating first-order reversal curve distributions using locally weighted regression smoothing, *Geochem. Geophys. Geosyst.,* **9,** Q05016, doi:10.1029/2008GC001987.

Hawthorne, T. & McKenzie, J., 1993. Biogenic magnetite: authigenesis and diagenesis with changing reodx conditions in lake Grweifen, Switzerland, in *Applications in Paleomagnetism to Sedimentary Geology,* pp. 3–15, eds Assaoui, D., McNeill, D. & Hurley, N.F., SEPM, Tulsa.

Horng, C.S. & Roberts, A.P., 2006. Authigenic or detrital origin of pyrrhotite in sediments? Resolving a paleomagnetic conundrum, *Earth planet. Sci. Lett.,* **241,** 750–762.

Itambi, A.C., von Dobeneck, T., Mulitza, S., Bickert, T. & Heslop, D., 2009. Millennial-scale northwest African droughts related to Heinrich events and Dansgaard-Oeschger cycles: evidence in marine sediments from offshore Senegal, *Paleoceanography,* **24,** PA1205, doi:10.1029/2007PA001570.

Jacobs, I.S., 1963. Metamagnetism of siderite ($FeCO_3$), *J. appl. Phys.*, **34,** 1106–1107.

Kakol, Z. & Honig, J.M., 1989. Influence of deviations from ideal stoichiometry on the anisotropy parameters of magnetite Fe3(1-δ)O4, *Phys. Rev.,* **40,** 9090–9097.

Kakol, Z., Sabol, J., Stickler, J. & Honig, J.M., 1992. Effect of low level titanium (IV) doping on the resistivity of magnetite near the Verwey transition, *Phys. Rev.,* **B46,** 1975–1978.

Kalu, A.E., 1979. The African dust Plume: its characteristics and propagation accross west Africa in winter, in *Saharan Dust: Mobilization, Transport, Deposition,* pp. 95–118, ed. Morales, C., Willey, New York.

Karlin, R., 1990. Magnetic mineral diagenesis in suboxic sediments at Bettis site W-N, NE Pacific ocean, *J. geophys. Res.,* **95**(B4), 4421–4436.

Karlin, R. & Levi, S., 1983. Diagenesis of magnetic minerals in recent hemipelagic sediments, *Nature,* **303,** 327–330.

Kato, H., Yamada, M., Yamauchi, H., Hiroyoshi, H., Takei, H. & Watanabe, H., 1982. Metamagnetic phase transitions in $FeTiO_3$, *J. Phys. Soc. Japan,* **51,** 1769–1777.

Kosterov, A., 2001. Magnetic properties of subaerial basalts at low temperatures, *Earth planet. Space,* **53,** 883–892.

Kruiver, P.P., Dekkers, M.J. & Heslop, D., 2001. Quantification of magnetic coercivity components by the analysis of acquisition curves of isothermal remanent magnetisation, *Earth planet. Sci. Lett.,* **189,** 269–276.

Lennie, A.R., England, K.E.R. & Vaughan, D.J., 1995. Transformation of synthetic mackinawite to hexagonal pyrrhotite: a kinetic study, *Am. Mineral.,* **80,** 960–967.

McCabe, C., Sassen, R. & Saffer, B., 1987. Occurrence of secondary magnetite within biodegraded crude oil, *Geology,* **15,** 7–10.

Morin, J., 1950. Magnetic susceptibility of α-Fe_2O_3 and Fe_2O_3 with added titanium, *Phys. Rev.,* **78,** 819–820.

Moskowitz, B.M. & Hargraves, R.B., 1984. Magnetic cristobalite: a possible new magnetic phase produced by the thermal decomposition of nontronite, *Science,* **225,** 1152–1154.

Moskowitz, B.M., Jackson, M. & Kissel, C., 1998. Low-temperature magnetic behaviour of titanomagnetites, *Earth planet. Sci. Lett.*, **157,** 141–149.

Mulitza, S. & cruise participants, 2006. Report and preliminary results of METEOR Cruise M65/1, Dakar-Dakar, 11.06–1.07.2005, Berichte, Fachbereich Geowissenschaften, Universität Bremen, No. 252, Bremen.

Mullender, T.A.T., van Velzen, A.J. & Dekkers, M.J., 1993. Continuous drift correction and separate identification of ferromagnetic and paramagnetic contributions in thermomagnetic runs, *Geophys. J. Int.,* **114,** 663–672.

Odin, G.S., 1975. Migration du fer des eaux continentales jusqu'aux eaux océaniques profondes, *C. R. Hedb. Seances Acad. Sci., Ser.,* **D281,** 1665–1668.

Özdemir, Ö., Dunlop, D.J. & Moskowitz, B.M., 1993. The effect of oxidation on the Verwey transition in magnetite, *Geophys. Res. Lett.*, **20,** 1671–1674.

Özdemir, Ö., Dunlop, D.J. & Berquó, T.S., 2008. Morin transition in hematite: size dependence and thermal hysteresis, *Geochem. Geophys. Geosyst.,* **9,** Q10Z01, doi:10.1029/2008GC002110.

Parkin, D.W., Sullivan, R.A.L. & Andrews, J.N., 1980. Further studies on cosmic spherules from deep-sea sediments, *Phil. Trans. R. Soc. Lond. A.,* **297,** 495–518.

Passier, H.F., Middelburg, J.J., de Lange, G.J. & Böttcher, M.E., 1999. Modes of sapropel formation in the eastern Mediterranean: some constraints based on pyrite properties, *Mar. Geol.,* **153,** 199–219.

Passier, H.F., de Lange, G.J. & Dekkers, M.J., 2001. Rock-magnetic properties and geochemistry of the active oxidation front and the youngest sapropel in the Mediterranean, *Geophys. J. Int.,* **145,** 604–614.

Petersen, N. & Vali, H., 1987. Observation of shrinkage cracks in ocean floor titanomagnetite, *Phys. Earth planet. Inter.,* **46,** 197–205.

Petersen, N., von Dobeneck, T. & Vali, H., 1986. Fossil bacterial magnetite in deep-sea sediments from the South Atlantic Ocean, *Nature,* **320,** 611–615.

Pike, C.R., Roberts, A.P. & Verosub, K.L., 1999. Characterizing interactions in fine magnetic particle systems using first order reversal curves, *J. appl. Phys.,* **85,** 6660–6667.

Pike, C.R., Roberts, A.P., Dekkers, M.J. & Verosub, K.L., 2001. An investigation of multi-domain hysteresis mechanisms using FORC diagrams, *Phys. Earth planet. Inter.,* **126,** 11–25.

Roberts, A.P., Pike, C.R. & Verosub, K.L., 2000. FORC diagrams: a new tool for characterizing the magnetic properties of natural samples, *J. geophys. Res.,* **105,** 28 461–28 475.

Rochette, P., Fillion, G., Mattéi, J.L. & Dekkers, M.J., 1990. Magnetic transition at 30–40 Kelvin in pyrrhotite: insight into a widespread occurrence of this mineral in rocks, *Earth planet. Sci. Lett*., **98,** 319–328.

Rognon, P., Coudé-Gaussen, G., Revel, M., Grousset, F.E. & Pédemay, P., 1996. Holocene Saharan dust deposition on the Cape Verde Islands: sedimentological and Nd–Sr isotopic arguments, *Sedimentology,* **43,** 359–366.

Rowan, C.J. & Roberts, A.P., 2006. Magnetite dissolution, diachronous greigite formation, and secondary magnetizations from pyrite oxidation:

unravelling complex magnetizations in Neogene marine sediments from New Zealand, *Earth planet. Sci. Lett.,* **241**(1–2), 119–137.

Sarnthein, M. & Koopmann B., 1979. Late quaternary deep-sea record on northwest African dust supply and wind circulation, *Paleoecol. Africa,* **12,** 239–253.

Sarnthein, M., Tetzlaff, G., Koopmann, B., Wolter, K. & Pflaumann, U., 1981. Glacial and interglacial wind regimes over the eastern subtropical Atlantic and Northwest Africa, *Nature,* **293,** 193–196.

Schwertmann, U., Cambier, Ph. & Murad, E., 1985. Properties of goethites of varying crystallinity, *Clays Clay Miner.,* **33,** 369–378.

Schwertmann, U., 1988. Occurrence and formation of iron oxides in various pedo- environments, in *Iron in Soils and Clay Minerals,* pp. 267–308, eds Stucki, J.W., Goodman, B.A., Schwertmann, U., Reidel, Dordrecht, the Netherlands.

Schoonen, M.A.A. & Barnes, H.L., 1991. Mechanisms of pyrite and marcasite formation from solution: III. Hydrothermal processes, *Geochim. Cosmochim. Acta.,* **55,** 3491–3504.

Smirnov, A.V. & Tarduno, J.A., 2000. Low-temperature magnetic properties of pelagic sediments (Ocean Drilling Program Site 805C): tracers of maghemitization and magnetic mineral reduction, *J. geophys. Res.,* **105**(2000), 16 457–16 471.

Stuut, J.B., Zabel, M., Ratmeyer, V., Helmke, P., Schefuß, E., Lavik, G. & Schneider, R., 2005. Provenance of present-day aeolian dust collected off NW Africa, *J. geophys. Res.,* **110,** doi:10.1029/2004JD005161.

Sun, W. & Jackson, M., 1994. Scanning electron microscopy and rock magnetic studies of magnetic carriers in remagnetized early Paleozoic carbonates from Missouri, *J. geophys. Res.* **99,** 2935–2942.

Suk, D., Peacor D.R. & Van Der Voo, R., 1990. Replacement of pyrite framboids by magnetite in limestone and implications for paleomagnetism, *Nature,* **345,** 611–613.

Sweeney, R.E. & Kaplan, I.R., 1973. Pyrite framboid formation: laboratory synthesis and marine sediments, *Econ. Geol.,* **68,** 618–634.

Syono, Y., 1965. Magneto-crystalline anisotropy and magnetostriction of Fe3O4-Fe2TiO4 series, with special application to rock magnetism, *Japan J. geophys.,* **4,** 71–143.

Taylor, G.R., 1982. A mechanism for framboid formation as illustrated by a volcanic exhalative sediment, *Miner. Depos.,* **17,** 23–36.

Van Velzen, A.J. & Dekkers, M.J., 1999. Low-temperature oxidation of magnetite in loess-paleosol sequences: a correction of rock magnetic parameters, *Stud. Geophys. Geod.,* **43,** 357–375.

Von Dobeneck, T., Petersen, N. & Vali, H., 1987. Bakteriële magnetofossilien, *Geowiss. in unserer Zeit,* **1,** 27–35.

Verwey, E.J., 1939. Electronic conduction of magnetite (Fe_3O_4) and its transition point at low temperatures, *Nature (London),* **144,** 327–328.

Wilkin, R.T. & Barnes, H.L., 1997. Formation processes of framboidal pyrite, *Geochim. Cosmochim. Acta.,* **61,** 323–339.